Large-momentum-transfer Bragg interferometer with strontium atoms

T. Mazzoni, X. Zhang,* R. Del Aguila, L. Salvi, N. Poli, and G. M. Tino†

Dipartimento di Fisica e Astronomia and LENS, Università di Firenze, INFN, Sezione di Firenze, Via Sansone 1, 50019 Sesto Fiorentino, Italy

(Received 24 June 2015; published 19 November 2015)

We report on an atom interferometer based on Bragg diffraction in a fountain of alkaline-earth-metal atoms, namely ^{88}Sr. We demonstrate large momentum transfer to the atoms up to eight photon recoils and the use of the interferometer as a gravimeter with a sensitivity $\delta g/g = 4 \times 10^{-8}$. Thanks to the special characteristics of strontium atoms for precision measurements, this result introduces alternate possibilities for experiments in fundamental and applied physics.

DOI: 10.1103/PhysRevA.92.053619 PACS number(s): 37.25.+k, 03.75.Dg, 91.10.Pp

I. INTRODUCTION AND MOTIVATION

Atom interferometers are rapidly evolving, being used as new quantum sensors for fundamental physics experiments and in several other applications [1]. In gravitational physics, for example, they enable precise measurements of gravity [2,3], gravity gradients [4,5], gravity curvature [6], and the Newtonian gravitational constant [7]. Important goals are the increase of their sensitivity and the demonstration of interferometry with atomic species other than alkali-metal atoms, which are most commonly used. For some experiments, indeed, the possibility of choosing the atomic species with the right characteristics is crucial. In particular, for precision measurements there is a considerable interest in using alkaline-earth-metal or alkaline-earth-metal-like atoms, such as Ca, Sr, or Yb [8–13], that are already used for the most advanced optical atomic clocks [14–17]. Alkaline-earth-metal atoms have several characteristics that make them particularly interesting in this context. First, their zero electronic angular momentum in the $^1S_0$ ground state makes these atoms less sensitive to perturbation due to magnetic fields than alkali-metal atoms. Furthermore, they offer more flexibility thanks to the presence of both dipole-allowed transitions and narrow intercombination transitions that can be used for efficient multiphoton Bragg diffraction [18–20] and for single-photon atom interferometry schemes [10,21]. Finally, resonance transitions from the ground state are in the blue/near-UV range (e.g., 461 nm for Sr, 399 nm for Yb), resulting in a larger momentum transferred to the atoms for the same diffraction order compared to alkali-metal atoms and hence in a correspondingly higher potential sensitivity of the interferometers.

Here, we demonstrate an atom interferometer based on large-momentum-transfer (LMT) Bragg diffraction in a fountain of alkaline-earth-metal atoms, namely strontium, and its use for the measurement of gravity acceleration. In addition to the general features of alkaline-earth-metal atoms listed above, the ^{88}Sr isotope that we use in this work has specific favorable characteristics: it has no nuclear spin so that in the ground state it is a scalar particle which is virtually insensitive to stray magnetic fields, and its small scattering length $a = -2a_0$ [22–24] results in reduced decoherence due to cold collisions. This allows, for example, observation of extremely long-lived Bloch oscillations of ^{88}Sr atoms in a vertical optical lattice [22,25]. On the other hand, since strontium has no hyperfine structure in the ground state, the usual schemes based on Raman transitions cannot be employed to realize the beam splitters and the mirrors for an interferometer. In this work, we use Bragg diffraction which, acting only on the atom's external degrees of freedom, can split the atomic wave packet into two momentum states separated by $2n\hbar k$ (where n is the Bragg diffraction order, and $k = 2\pi/\lambda$ is the wave vector of the Bragg laser light with a wavelength λ), while maintaining the same electronic state.

II. METHOD AND EXPERIMENTAL SETUP

In Fig. 1(a), a schematic view of the experimental apparatus is shown. The beams at 461 nm for the Bragg transitions are produced by a home-made laser that is frequency-locked to the main cooling laser with a red detuning Δ which is set, for different Bragg orders, in the 3–8 GHz range with respect to the $^1S_0$-$^1P_1$ transition frequency. The output power is about 200 mW and the emission linewidth is about 1 MHz. The laser intensity is actively stabilized using an external single-pass acousto-optical modulator (AOM) (see the Appendix for details on the noise spectrum). The two Bragg beams, with frequencies ω_1 and ω_2, are obtained using two separate AOMs and they are coupled with mutually orthogonal polarizations into a single-mode polarization-maintaining fiber. They are collimated at a $1/e^2$ intensity radius of $r = 2.5$ mm and sent vertically upwards onto the atomic sample. The light is then retroreflected by a 2-in. mirror suspended on a vibration isolation platform (MinusK 25BM-4). A quarter-wave plate is placed before the retroreflection mirror to rotate the polarization of the returning light by 90°. This allows the beams to interfere with each other to generate two traveling waves moving in opposite directions, while the formation of standing waves by pairs of beams with the same frequency is avoided. The difference between the beams' frequencies $\delta_n = \omega_1 - \omega_2$ is adjusted in order to have the upward-moving lattice drive the Bragg transitions, which occur for $\delta_n = 4n\omega_r$ in the falling frame, where $\omega_r = \hbar k^2/2m = 2\pi \times 10.7$ kHz is the recoil frequency for strontium atoms. The lattice moving downward is Doppler shifted out of resonance during most of the atoms' free fall. Bragg pulses at the apogee of the ballistic trajectories are avoided to prevent double

*Also at International Centre for Theoretical Physics (ICPT), Trieste, Italy.

†Guglielmo.Tino@fi.infn.it

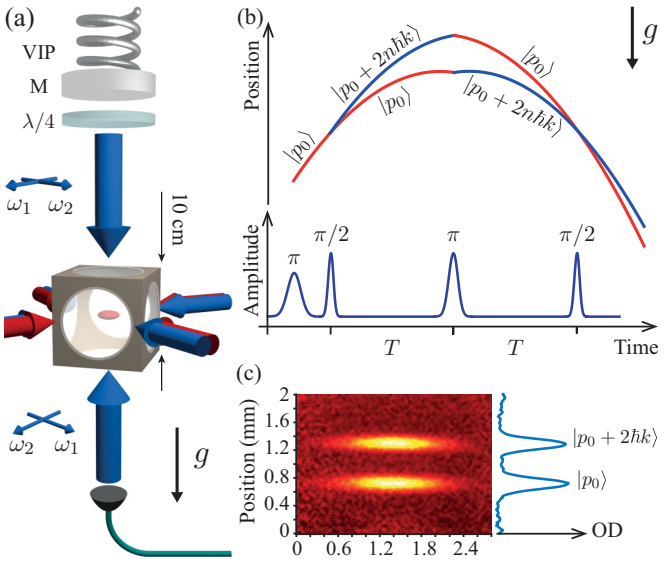

FIG. 1. (Color online) (a) Simplified picture of the experimental apparatus. The ^{88}Sr atoms are cooled in a double-stage magneto-optical trap. The Bragg laser beams with frequencies ω_1 and ω_2 and orthogonal polarizations are sent vertically from the bottom of the chamber, rotated by a $\lambda/4$ wave plate and retroreflected by a mirror (M) installed on a vibration isolation platform (VIP). (b) Scheme of the atom interferometer with separated arms corresponding to different momentum states under the effect of gravity. Before the interferometric sequence the atoms are velocity selected and launched by a sequence of π pulses. (c) Time-of-flight image ($T_{\rm tof} = 30$ ms) of the two interferometer arms split by a first-order $\pi/2$ pulse. The spatial separation after 30 ms is 600 μm.

diffraction. The verticality of the beam is verified at 1 mrad by retroreflecting it on a water surface. The residual vibrations and tilt coupled to the retroreflecting mirror are monitored by a triaxial accelerometer (Episensor ES-T) and a precision tiltmeter (Applied Geomechanics Tuff Tilt 420) placed on top of the vibration-isolation platform (see the Appendix for details on noise spectra). The whole platform is enclosed in an acoustic isolation box. The two Bragg AOMs are driven by two rf generators phase-locked to a 10-MHz reference signal provided by a Rb clock and the pulses are shaped to have a Gaussian profile [26] using an additional signal generator that drives two variable attenuators acting on both the rf Bragg signals. The phase noise of the Bragg beams in this configuration was characterized with a digital phase detector by comparing the beat note of the two frequency components detected on a photodiode (placed after the optical fiber) with a reference rf synthesizer (see Appendix).

With an available optical power on the atoms of $P = 20$ mW per beam, the typical optical intensity is $I = 250$ mW/cm^2 and the maximum two-photon Rabi frequency estimated for Gaussian pulses at a detuning $\Delta = 8$ GHz is $\Omega = 2\pi \times 150$ kHz. For different Bragg orders the detuning is adjusted to maintain a high effective Rabi frequency $\Omega_{\rm eff} = \Omega^n/[(8\omega_r)^{n-1}(n-1)!^2]$ [27]. The pulse duration is kept larger than $n^{1/6}[\omega_r(n-1)]$ to ensure that the losses into other orders remain negligible [26] and thus guarantee high π-pulse efficiencies. We set a typical effective Rabi frequency $\Omega_{\rm eff} = 2\pi \times 80$ kHz, with a π pulse duration of 15 μs full width at half maximum (FWHM), corresponding to a Fourier width larger than the atoms' momentum spread. At a detuning $\Delta = 2.8$ GHz and full power, we obtain a diffraction efficiency of 50% for the fourth order.

The experimental sequence is the following: ^{88}Sr atoms from an atomic beam produced using a high-efficiency oven [28] are decelerated in a Zeeman slower and then trapped and cooled in a two-stage magneto-optical trap (MOT). The first "blue" MOT is realized using the strong $^1S_0$-$^1P_1$ transition at 461 nm to reach a temperature of 1 mK. The atoms are then further cooled in a "red" MOT operating on the narrow intercombination $^1S_0$-$^3P_1$ transition at 689 nm, reaching a final temperature of 1.2 μK, with a spatial radial (vertical) size of 300 μm (50 μm) FWHM. The sequence produces about 2×10^6 trapped atoms in 1.5 s. A small fraction of the atoms ($\sim 10^5$) is selected from the MOT and launched upwards with a sequence of Bragg π pulses with a typical duration of 47 μs FWHM, up to a total momentum transfer of 40 $\hbar k$. Even though a single π pulse would be sufficient to isolate the selected atoms from the freely falling cloud after the release from the red MOT, a larger number of pulses is applied to increase the total time of flight up to 150 ms. By means of Bragg spectroscopy [29] we estimate a vertical momentum spread of $1.5\hbar k$ FWHM for the red MOT, and $0.2\hbar k$ for the selected atomic sample, which allows high fidelity π and $\pi/2$ pulses in the interferometer [30]. Incidentally, in this work we also performed preliminary tests of velocity selection and launch of Sr atoms in a fountain using Bloch oscillations in an accelerated vertical optical lattice at 532 nm. After the launch of the atoms in the fountain, a Mach-Zehnder interferometer is realized by applying three Bragg pulses in a $(\pi/2)$-π-$(\pi/2)$ configuration. As shown in Fig. 1(b), the first $\pi/2$ pulse coherently splits the atomic wave packet over two paths separated by $2n\hbar k$. Figure 1(c) shows an image of the atoms in the two arms of the interferometer after 30 ms for a first-order pulse. The spatial separation between the two interferometer arms is 600 μm, which is about two times larger than the separation induced by near-infrared light in alkali-metal-atom interferometers. The two paths in the interferometer are recombined after a time $2T$. The population in the two output ports is detected by either absorption imaging or fluorescence collection about 40 ms after the last pulse is applied, when the two momentum states are sufficiently separated in space. The interferometer time T is currently limited by the vertical size of the vacuum chamber (10 cm), which limits the total time of flight for the atoms in the fountain.

The number of atoms in the two outputs, $N_{|p_0\rangle}$ and $N_{|p_0+2n\hbar k\rangle}$, is determined by fitting the detected signal with two Gaussian profiles. They oscillate periodically as a function of the relative phase Φ acquired by the atoms in the two arms. The output signal of the interferometer $P(\Phi)$ is given by the relative population

$$P(\Phi) = \frac{N_{|p_0\rangle}}{N_{|p_0\rangle} + N_{|p_0+2n\hbar k\rangle}} = P_0 + \frac{C}{2}\cos(\Phi), \qquad (1)$$

where $P_0 \sim 0.5$ is an offset and C is the contrast. For a vertical Mach-Zehnder Bragg interferometer, the relative phase depends on the gravity acceleration g, the effective laser wave number $2nk$, the interferometer time T, and the optical

phase of the Bragg pulses:

$$\Phi = n(2kg - \alpha)T^2 + n(\phi_1 - 2\phi_2 + \phi_3), \tag{2}$$

where $\alpha = 2\pi \times 42.5509$ kHz/ms is a frequency chirping applied to the Bragg beams in order to compensate for the varying Doppler shift of the falling atoms, and ϕ_i is the relative phase between the two beams for the ith pulse.

III. EXPERIMENTAL RESULTS AND DISCUSSION

A. Contrast

The contrast of the interference fringes, obtained by scanning the phase ϕ_3 of the last $\pi/2$ pulse, was determined from the values of $P(\Phi)$ between the 2nd and the 98th percentile [31]. Figure 2 shows the values of the observed contrast for first, second, and third Bragg order as a function of the interferometer time T. For different orders, the Bragg laser detuning Δ was chosen in order to maintain a high Rabi frequency and a low rate of light scattering, according to the available laser power. For short interferometer times, the contrast is mainly limited by the velocity spread along the vertical direction and by the residual light scattering, which limits the π-pulse efficiency. For long interferometer times, the contrast is mainly limited by the Rabi frequency inhomogeneity which is due to both the radial expansion of the atomic cloud and the intensity profile imperfections of the Bragg beams [20,32]. The sensitivity to this inhomogeneity becomes more critical as the Bragg order n increases because the effective Rabi frequency scales as the nth power of the two-photon Rabi frequency. This shows that the small sample size and the ultralow temperatures achievable with strontium atoms can lead to a high contrast for long interferometer times even with relatively narrow Bragg beams. Further improvement in the contrast can be obtained by reducing the probe beam size in order to only interact with the central atoms, for which the Rabi frequency inhomogeneities due to the transverse expansion are smaller. However, in doing this the effect on the sensitivity has to be taken into account. Reducing the interrogation area will reduce the number of interrogated atoms, leading to an increase of the shot-noise limit and of detection noise. Therefore, there is a trade-off between contrast gain and noise suppression which has to be optimized in order to really improve the sensitivity of the gravimeter. Conversely, it is possible to explore geometries where the atoms are guided by a dipole trap along the falling axis. In this scenario the atoms could be forced to remain in the region of maximum intensity of the Bragg beams, ensuring that they all contribute to the interferometer signal. A technically feasible improvement by an order of magnitude in the Bragg laser power would allow us to move further from resonance ($\Delta \sim 600\Gamma$) maintaining a sufficiently high Rabi frequency and therefore realize a higher-order interferometer as demonstrated for Cs [20].

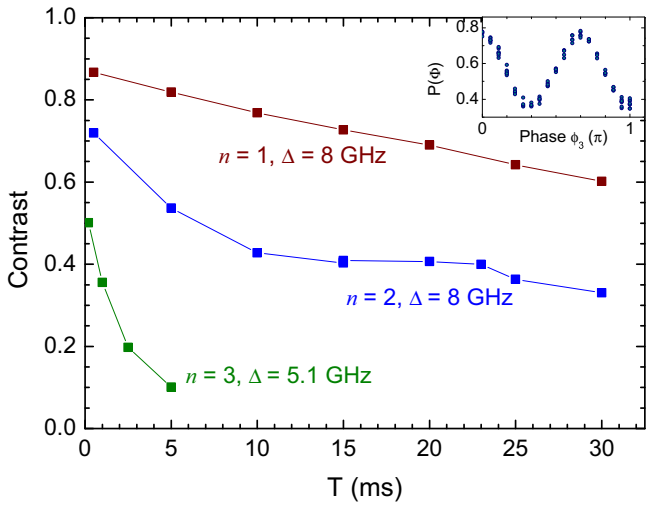

FIG. 2. (Color online) Contrast of the interference fringes as a function of time T for first-, second-, and third-order Bragg diffraction with detuning Δ. The inset shows a typical fringe observed at $T = 0.2$ ms for a third-order Bragg interferometer.

B. Sensitivity

The sensitivity $\delta g/g$ of the interferometer as a gravimeter is determined by measuring the phase fluctuations $\delta\Phi$ at the slope of the central fringe:

$$\frac{\delta g}{g} = \frac{\delta\Phi}{2nkgT^2}. \tag{3}$$

The short- and long-term sensitivities are characterized with the Allan deviation. The results for a first-order interferometer with a time $T = 30$ ms and the estimated effect of the main noise sources are shown in Fig. 3. The Allan deviation scales as the inverse root of the integration time with $\delta g/g = 1.5 \times 10^{-6}$ at 1 s, reaching 4×10^{-8} at 2000 s. The sensitivity of our interferometer is presently limited by the residual acceleration

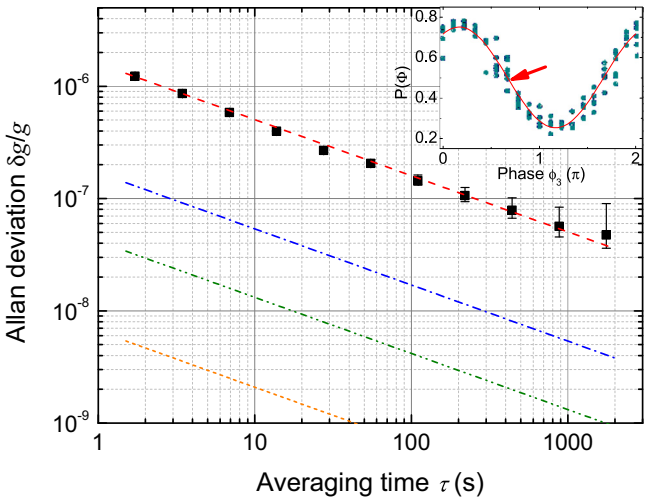

FIG. 3. (Color online) Allan deviation of the gravity acceleration measurements for a first-order interferometer with a time $T = 30$ ms (black squares). The inset shows the corresponding fringe and the point at which the phase fluctuations are measured. Also shown in the figure are the estimated effects due to the residual acceleration noise of the retroreflection mirror (dashed red line), the optical phase noise of the Bragg beams (dash-dotted blue line), the intensity noise of the Bragg beams (short-dashed orange line), and the shot noise (1×10^5 atoms, dash-dot-dotted green line).

of the suspended retroreflection mirror. The estimated phase noise due to the mirror vibrations is 380 mrad/$\sqrt{\tau}$, where τ is the averaging time. The second major noise contribution comes from the optical phase noise of the Bragg beams, which is estimated to be 20 mrad/$\sqrt{\tau}$, more than one order of magnitude smaller than the vibration noise. The calculated phase noise arising from intensity fluctuations of the Bragg laser is 1 mrad/$\sqrt{\tau}$, while other noise sources such as ac Stark shift effects and Bragg frequency noise are estimated to give contributions below the μrad/$\sqrt{\tau}$ level (see the Appendix). Finally, the shot-noise limit for 1×10^5 atoms is 10 mrad/$\sqrt{\tau}$.

IV. CONCLUSIONS AND OUTLOOK

In conclusion, we demonstrated LMT Bragg interferometry in a fountain of alkaline-earth-metal atoms for the first time. The results are mainly limited by technical aspects such as the available laser power, the size of the vacuum cell, and residual vibrations; therefore, we anticipate a dramatic increase in performance with the increasing power of available lasers, a larger chamber to increase the interferometer time, and improved isolation from vibrational noise. A variation on our scheme is the possibility to induce the Bragg transitions using the narrow intercombination line at 689 nm where stable lasers with a higher output power are already available. Moreover, schemes based on the combination of Bragg diffraction and Bloch oscillations [33–35] might allow superior performance in terms of precision and accuracy thanks to the specific properties of strontium. Other relevant prospects are the use of ultracold Sr sources [36] and high-sensitivity detection schemes beyond the classical limit [37].

In order to surpass present limits and take full advantage of the methods and ideas discussed in this paper, we are developing an apparatus for a large-scale (∼10-m-high) Sr fountain. Possible fundamental physics experiments include stringent tests of the Einstein equivalence principle and possible spin-gravity coupling [11,25], tests of models of quantum gravity [38] and dark matter [39], new schemes to determine the value of the gravitational constant [40], and the detection of gravitational waves [41]. Potential applications in geophysics and geodesy can also be envisaged [42].

In the long term, a space mission based on strontium atoms combining atom interferometers and transportable optical clocks [43] together with a suitable configuration for gravitational wave detection [10,21] would enable extremely high precision tests of different fundamental aspects of gravitational physics [40,44].

ACKNOWLEDGMENTS

We acknowledge support by INFN and the Italian Ministry of Education, University and Research (MIUR) under the Progetto Premiale "Interferometro Atomico" and by LENS. We also acknowledge support from the European Union's Seventh Framework Programme (FP7/2007-2013 Grant No. 250072, the "iSense" project, and FP7-PEOPLE-2013-ITN Grant No. 607493, the "FACT" project). We thank G. Rosi for useful discussions.

APPENDIX: MAIN NOISE SOURCES IN THE Sr INTERFEROMETER

Here we provide evaluation of the main noise sources limiting the sensitivity of the Sr interferometer. The measured typical power spectral noise densities (PSDs) are also reported. Here, all the equations for the noise estimation are written for first-order Bragg diffraction, $n = 1$. It must be noted that, while the estimated phase noise is proportional to n, the sensitivity of the interferometer [$\delta g/g$, as given by the Eq. (3) in the main text] does not depend on n. For the evaluation, we have considered the following typical interferometer parameter values: interferometer time $T = 30$ ms, cycle time $T_c = 1.7$ s, and $\pi/2$ Bragg pulse duration $\tau_B = 10$ μs. In order to maintain simplicity in the calculations we consider Bragg pulses with a square profile, although a Gaussian profile is used in the experiment. What is important for the evaluation of the noise contributions is actually the pulse area $\tau_B \Omega_R$ and, therefore, for $\tau_B \ll T$, using different pulse shape has a negligible effect on the result.

Figure 4(a) shows the PSD measurement of the Bragg laser intensity noise. The estimation of phase shift induced on the interferometer by this noise follows the analysis done for Raman interferometers (see, for example, [45]). The phase noise, written in terms of its Allan variance, is given by the following formula:

$$\sigma^2_{\Phi,I}(\tau) = \frac{T_c}{\tau} \int_0^{+\infty} S_I(f) |H_I(f)|^2 df, \qquad \text{(A1)}$$

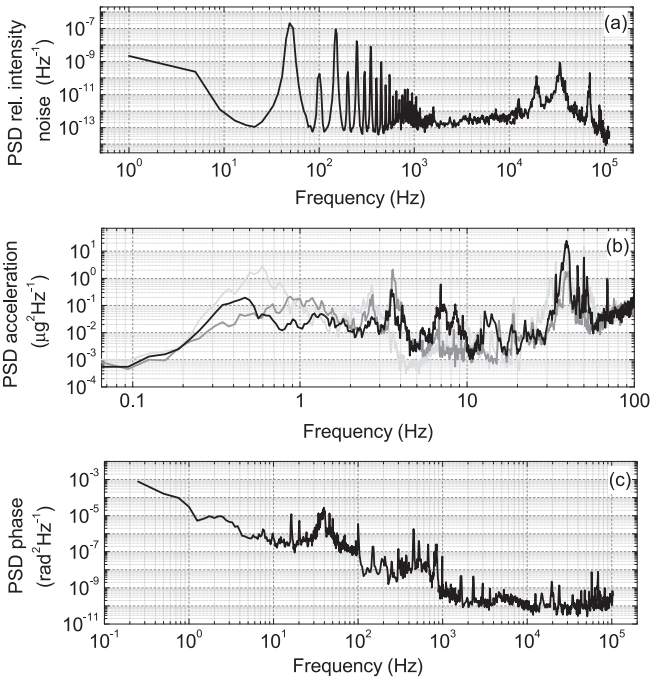

FIG. 4. Power spectral densities of main noise sources contributing to Sr interferometer phase noise: (a) PSD of relative intensity noise of the 461-nm Bragg laser; (b) PSD of acceleration noise measured on top of the MinusK platform on which is rigidly mounted the retroreflecting mirror for the Bragg beams, along three orthogonal axes: vertical (black), horizontal east (dark gray), and horizontal north (light gray); and (c) PSD of phase noise of the Bragg pulses.

where the sensitivity function $H_I(f)$ is given by

$$|H_I(f)|^2 = \frac{\sqrt{3}\pi}{C}\frac{\sin^4(2\pi fT)}{(2\pi fT)^2}, \tag{A2}$$

where C is the contrast of the interferometer. For our selected values we estimate a $\sigma_{\Phi,I}(\tau) = 1\ \text{mrad}/\sqrt{\tau}$.

The PSD measurement of the phase noise $S_\phi(f)$ on the Bragg beams is presented in Fig. 4(c). This has been characterized through the use of a digital phase and frequency detector (PFD) by comparing the beat note of the two Bragg frequency components, ω_1 and ω_2, to a reference rf synthesizer. The beat note is detected on a photodiode placed after the polarization-maintaining fiber (just before the atomic sample). The integrated phase noise on a time scale of 100 ms is 1 mrad. Under our typical conditions we estimate $\sigma_{\Phi,\phi}(\tau) = 20\ \text{mrad}/\sqrt{\tau}$, according to the standard formula [46,47]

$$\sigma^2_{\Phi,\phi}(\tau) = \frac{T_c^2}{\tau^2}\int_0^{+\infty}\frac{4\sin^4(\pi f\tau)}{\sin^2(\pi fT_c)}|H_\phi(f)|^2 S_\phi(f)df, \tag{A3}$$

where the transfer function $H_\phi(f)$ is given, as usual, by the Fourier transform of the sensitivity function $g(t)$:

$$H_\phi(f) = 2\pi f\int_{-\infty}^{+\infty} e^{i2\pi ft}g(t)dt. \tag{A4}$$

The sensitivity function $g(t)$ for a sequence of three pulses $(\pi/2)$-π-$(\pi/2)$ of duration τ_B-$2\tau_B$-τ_B separated by a time T with Rabi frequency Ω_R is

$$g(t) = \begin{cases} 0 & \text{for } -T_c/2 < t < -T, \\ \sin[\Omega_R(t+T)] & \text{for } -T < t < -T+\tau_B, \\ 1 & \text{for } -T+\tau_B < t < -\tau_B, \\ -\sin[\Omega_R t] & \text{for } -\tau_B < t < \tau_B, \\ -1 & \text{for } \tau_B < t < T-\tau_B, \\ \sin[\Omega_R(t-T)] & \text{for } T-\tau_B < t < T, \\ 0 & \text{for } T < t < T_c/2. \end{cases}$$

Another important contribution to the interferometer noise is the vibration noise, which is directly coupled to the upper retroreflecting mirror for the Bragg beams. The PSD of acceleration noise $S_a(f)$, measured on top of the supporting MinusK platform, is shown in Fig. 4(b). The degradation to the Sr interferometer sensitivity due to vibrations coupled to the retroreflecting Bragg mirror has been evaluated with the formula [46,47]

$$\sigma^2_{\Phi,a}(\tau) = \frac{k_{\text{eff}}^2}{\tau}\sum_{n=1}^{\infty}\frac{|H(2\pi nf_c)|^2}{(2\pi nf_c)^4}S_a(2\pi nf_c). \tag{A5}$$

Here $k_{\text{eff}} = 2k = 4\pi/\lambda$ is the effective wave vector of the first-order Bragg diffraction with $\lambda = 461$ nm. For our typical vibration noise, we estimated an Allan deviation of $\sigma_{\Phi,a}(\tau) = 380\ \text{mrad}/\sqrt{\tau}$. This contribution sets the actual limit on our interferometer sensitivity.

Intensity fluctuations of the Bragg laser could, in principle, induce phase noise through the ac Stark shift effect. However, for Bragg diffraction this effect is reduced in comparison to Raman interactions, since atoms remain in the same internal state and only their momentum changes. A residual differential shift comes from the different detunings for the two momentum states through the Doppler shift effect. One should therefore still expect a small contribution to phase noise proportional to the intensity fluctuation [19]:

$$\Delta\phi_{\text{ac}} = \frac{4\delta}{\Delta}\frac{\delta I}{I}, \tag{A6}$$

where δ and Δ are the Bragg resonance frequency and the Bragg laser detuning, respectively, and δI is the intensity fluctuation over the interferometer time. With our typical parameters, we estimate an induced phase noise of 4 μrad per shot, which is negligible compared to other sources of noise.

Finally, the influence of fluctuations of the absolute Bragg laser wave vector has also been estimated. For this, the frequency stability of the 461-nm Bragg laser has been characterized through the beat note of the Bragg laser against the master cooling laser at 461 nm. The relative frequency instability at 1 s is 7×10^{-10}, indicating a relative uncertainty of 7×10^{-10} on g, based on the relation

$$\frac{\Delta g}{g} = \frac{\Delta k_{\text{eff}}}{k_{\text{eff}}} = \frac{\Delta\nu}{\nu}. \tag{A7}$$

In conclusion, the absolute frequency noise of the Bragg laser is not currently limiting the performance of the interferometer.

[1] *Atom Interferometry*, in Proceedings of the International School of Physics "Enrico Fermi," Course CLXXXVIII, Varenna, 2013, edited by G. M. Tino and M. A. Kasevich (Società Italiana di Fisica and IOS Press, Amsterdam, 2014).

[2] A. Peters, K. Chung, and S. Chu, Nature (London) **400**, 849 (1999).

[3] P. Gillot, O. Francis, A. Landragin, F. P. Dos Santos, and S. Merlet, Metrologia **51**, L15 (2014).

[4] J. M. McGuirk, G. T. Foster, J. B. Fixler, M. J. Snadden, and M. A. Kasevich, Phys. Rev. A **65**, 033608 (2002).

[5] F. Sorrentino, Q. Bodart, L. Cacciapuoti, Y.-H. Lien, M. Prevedelli, G. Rosi, L. Salvi, and G. M. Tino, Phys. Rev. A **89**, 023607 (2014).

[6] G. Rosi, L. Cacciapuoti, F. Sorrentino, M. Menchetti, M. Prevedelli, and G. M. Tino, Phys. Rev. Lett. **114**, 013001 (2015).

[7] G. Rosi, F. Sorrentino, L. Cacciapuoti, M. Prevedelli, and G. M. Tino, Nature (London) **510**, 518 (2014).

[8] F. Riehle, T. Kisters, A. Witte, J. Helmcke, and C. J. Bordé, Phys. Rev. Lett. **67**, 177 (1991).

[9] M. G. Tarallo, N. Poli, M. Schioppo, D. Sutyrin, and G. M. Tino, Appl. Phys. B **103**, 17 (2011).

[10] P. W. Graham, J. M. Hogan, M. A. Kasevich, and S. Rajendran, Phys. Rev. Lett. **110**, 171102 (2013).

[11] M. G. Tarallo, T. Mazzoni, N. Poli, D. V. Sutyrin, X. Zhang, and G. M. Tino, Phys. Rev. Lett. **113**, 023005 (2014).

[12] A. O. Jamison, B. Plotkin-Swing, and S. Gupta, Phys. Rev. A **90**, 063606 (2014).

[13] J. Hartwig, S. Abend, C. Schubert, D. Schlippert, H. Ahlers, K. Posso-Trujillo, N. Gaaloul, W. Ertmer, and E. M. Rasel, New J. Phys. **17**, 035011 (2015).

[14] N. Hinkley, J. A. Sherman, N. B. Phillips, M. Schioppo, N. D. Lemke, K. Beloy, M. Pizzocaro, C. W. Oates, and A. D. Ludlow, Science **341**, 1215 (2013).
[15] I. Ushijima, M. Takamoto, M. Das, T. Ohkubo, and H. Katori, Nat. Photonics **9**, 185 (2015).
[16] B. J. Bloom, T. L. Nicholson, J. R. Williams, S. L. Campbell, M. Bishof, X. Zhang, W. Zhang, S. L. Bromley, and J. Ye, Nature (London) **506**, 71 (2014).
[17] N. Poli, C. W. Oates, P. Gill, and G. M. Tino, Riv. Nuovo Cimento **36**, 555 (2013).
[18] D. M. Giltner, R. W. McGowan, and S. A. Lee, Phys. Rev. Lett. **75**, 2638 (1995).
[19] P. A. Altin, M. T. Johnsson, V. Negnevitsky, G. R. Dennis, R. P. Anderson, J. E. Debs, S. S. Szigeti, K. S. Hardman, S. Bennetts, G. D. McDonald, L. D. Turner, J. D. Close, and N. P. Robins, New J. Phys. **15**, 023009 (2013).
[20] H. Müller, S.-w. Chiow, Q. Long, S. Herrmann, and S. Chu, Phys. Rev. Lett. **100**, 180405 (2008).
[21] N. Yu and M. Tinto, Gen. Relativ. Gravitation **43**, 1943 (2011).
[22] G. Ferrari, R. E. Drullinger, N. Poli, F. Sorrentino, and G. M. Tino, Phys. Rev. A **73**, 023408 (2006).
[23] Y. N. Martinez de Escobar, P. G. Mickelson, P. Pellegrini, S. B. Nagel, A. Traverso, M. Yan, R. Côté, and T. C. Killian, Phys. Rev. A **78**, 062708 (2008).
[24] A. Stein, H. Knöckel, and E. Tiemann, Eur. Phys. J. D **57**, 171 (2010).
[25] N. Poli, F.-Y. Wang, M. G. Tarallo, A. Alberti, M. Prevedelli, and G. M. Tino, Phys. Rev. Lett. **106**, 038501 (2011).
[26] H. Müller, S.-w. Chiow, and S. Chu, Phys. Rev. A **77**, 023609 (2008).
[27] D. M. Giltner, R. W. McGowan, and S. A. Lee, Phys. Rev. A **52**, 3966 (1995).
[28] M. Schioppo, N. Poli, M. Prevedelli, S. Falke, C. Lisdat, U. Sterr, and G. M. Tino, Rev. Sci. Instrum. **83**, 103101 (2012).
[29] J. Stenger, S. Inouye, A. P. Chikkatur, D. M. Stamper-Kurn, D. E. Pritchard, and W. Ketterle, Phys. Rev. Lett. **82**, 4569 (1999).
[30] S. S. Szigeti, J. E. Debs, J. J. Hope, N. P. Robins, and J. D. Close, New J. Phys. **14**, 023009 (2012).
[31] G. D. McDonald, H. Keal, P. A. Altin, J. E. Debs, S. Bennetts, C. C. N. Kuhn, K. S. Hardman, M. T. Johnsson, J. D. Close, and N. P. Robins, Phys. Rev. A **87**, 013632 (2013).
[32] G. D. McDonald, C. C. N. Kuhn, S. Bennetts, J. E. Debs, K. S. Hardman, M. Johnsson, J. D. Close, and N. P. Robins, Phys. Rev. A **88**, 053620 (2013).
[33] T. Kovachy, J. M. Hogan, D. M. S. Johnson, and M. A. Kasevich, Phys. Rev. A **82**, 013638 (2010).
[34] H. Müller, S.-w. Chiow, S. Herrmann, and S. Chu, Phys. Rev. Lett. **102**, 240403 (2009).
[35] R. Charrière, M. Cadoret, N. Zahzam, Y. Bidel, and A. Bresson, Phys. Rev. A **85**, 013639 (2012).
[36] S. Stellmer, R. Grimm, and F. Schreck, Phys. Rev. A **87**, 013611 (2013).
[37] M. A. Norcia and J. K. Thompson, arXiv:1506.02297.
[38] G. Amelino-Camelia, C. Lämmerzahl, F. Mercati, and G. M. Tino, Phys. Rev. Lett. **103**, 171302 (2009).
[39] P. Hamilton, M. Jaffe, P. Haslinger, Q. Simmons, H. Müller, and J. Khoury, Science **349**, 849 (2015).
[40] G. M. Tino, in *Atom Interferometry*, Proceedings of the International School of Physics "Enrico Fermi," Course CLXXXVIII, Varenna, 2013 (Società Italiana di Fisica and IOS Press, Amsterdam, 2014), p. 457.
[41] G. M. Tino, F. Vetrano, and C. Lämmerzahl, Gen. Relativ. Gravitation (special issue) **43**, 1901 (2011).
[42] M. de Angelis, A. Bertoldi, L. Cacciapuoti, A. Giorgini, G. Lamporesi, M. Prevedelli, G. Saccorotti, F. Sorrentino, and G. M. Tino, Meas. Sci. Technol. **20**, 022001 (2009).
[43] N. Poli, M. Schioppo, S. Vogt, S. Falke, U. Sterr, Ch. Lisdat, and G. M. Tino, Appl. Phys. B **117(4)**, 1107 (2014).
[44] G. M. Tino, L. Cacciapuoti, K. Bongs, C. J. Bordé, P. Bouyer, H. Dittus, W. Ertmer, A. Görlitz, M. Inguscio, A. Landragin, P. Lemonde, C. Lammerzahl, A. Peters, E. Rasel, J. Reichel, C. Salomon, S. Schiller, W. Schleich, K. Sengstock, U. Sterr, and M. Wilkens, Nucl. Phys. B, Proc. Suppl. **166**, 159 (2007).
[45] A. Peters, Ph.D thesis, Stanford University, 1998 (unpublished).
[46] J. Le Gouët, T. E. Mehlstäubler, J. Kim, S. Merlet, A. Clairon, A. Landragin, and F. Pereira Dos Santos, Appl. Phys. B **92**, 133 (2008).
[47] P. Cheinet, B. Canuel, F. Pereira Dos Santos, A. Gauguet, F. Leduc, and A. Landragin, IEEE Trans. Instrum. Meas. **57**, 1141 (2008).